Differences in the sulfate-methane transitional zone in coastal pockmarks in various sedimentary environments

Chao Cao[1,2,3]*, Feng Cai[1,2], Hongshuai Qi[1,2,3], Shaohua Zhao[1], Chengqiang Wu[1]

1 Third Institute of Oceanography, Ministry of Natural Resources, Xiamen, China

2 Fujian Provincial Key Laboratory of Marine Ecological Conservation and Restoration, Xiamen, China

3 Fujian Provincial Station for Field Observation and Research of Island and Costal Zone in Zhangzhou, Xiamen, China

* Correspondence: caochao@tio.org.cn; Tel: +86-592-2195306

Abstract: Different types of pockmarks, including single pockmarks, circular pockmarks, elongated pockmarks, chain-type pockmarks and compound pockmarks, were identified in coastal areas around Fujian, China. The sediments associated with pockmarks were mainly silty clay to clay, with a small quantity of silt with fine sand. The sulfate content in the pore water in the sedimentary layers associated with pockmarks decreased with depth from the surface, whereas the free methane content increased with depth. The interaction between sulfate and methane is well known, but differences in the sulfate-methane transitional zone (SMTZ) were observed in different areas with different hydrologic characteristics. The sedimentary SMTZ of the offshore Zhe-min mud wedge was shallow, at 50–70 cm below the seafloor. The sedimentary SMTZ was moderately deep (90–115 cm) in the central bay area and deep (180–200 cm) in the sandy area offshore. This variability in SMTZ depth reflects different amounts of free methane gas in the underlying formations, with a shallower SMTZ indicating a higher free methane content. The free methane had $\delta^{13}C$ values of -26.47‰ to -8.20‰ and a biogenic-hybrid genetic type. The flux of sedimentary gas from the pockmark surfaces, calculated according to Fick's formula, was 2.89 to 18.85 $l/m^2 \cdot a$. The shape, size and scale of the pockmarks are directly related to the substrate type and the gas production of the underlying strata and thus vary with the sedimentary environment and development stage. Therefore, different types of pockmarks, in various phases of development, are associated with different

sedimentary and dynamical conditions. A single circular pockmark forms by strong methane flux. As the intensity of methane flux weakens, the pockmark becomes elongated in the direction of the water flow because of long-term erosion induced by regular hydrodynamic forces. Finally, under weak intensity of methane flux and the influence of complex hydrodynamic conditions, pockmarks merge to form large-scale, compound pockmarks.

Keywords: pockmark; sulfate and methane transitional zone; various sedimentary environments; pore water and sediment

1. Introduction

Submarine pockmarks were first discovered in 1970 during a submarine oil and gas exploration process on the continental shelf of Nova Scotia in Canada [1]. However, these crater-shaped submarine depressions did not become widely known. It was not until 1987 that Hovland reported features described as hemp pits in North Sea sediments in authigenic carbonate cement and confirmed that pockmarks formation was related to methane leakage events. Researchers gradually realized that pockmarks may indicate past and present submarine fluid activity. With the development of seismic exploration technology and marine acoustic detection technology, an increasing number of submarine pockmarks have been found globally, such as on the continental slope of northern Norway, the continental slope of equatorial West Africa, the Bering Sea, the North Sea, the continental shelf of western Canada, the Gulf of Mexico, the Black Sea, the East China Sea and the South China Sea [2-9]. Due to complexities and differences in the marine environments and submarine fluid activities, pockmarks show different sizes, morphological characteristics, distribution locations and water depths. Moreover, the biogeochemistry of the pockmark sediments can also indicate the formation environment of the pockmarks [10].

It is well known that a large quantity of sulfate is a major component of sedimentary pore waters in the early stages of sediment formation in estuarine and offshore areas [11-15]. Through the decomposition of sedimentary organic matter and resulting increase in the methane concentration, pore water sulfate concentrations decrease over time [16-19]. This can also lead to abnormal chloride concentrations

and oxygen and hydrogen isotope values, and these anomalous values can be used to differentiate various sedimentary environments [20-23]. A sharp linear reduction in pore water sulfate concentrations and a relative shallow sulfate-methane transitional zone (SMTZ) reflect a high intensity of methane flux through the underlying sedimentary layers and suggest an anoxic sedimentary environment [8,24,25]. Thus, sulfate and halide concentrations, a high intensity of methane flux, authigenic carbonate minerals and other geochemical indicators are significant factors in studies on early diagenesis and the sedimentary environment [26-28]. Estuaries and coasts are the convergence zones of the land and sea, into which large amounts of terrestrial organic matter are input every year [29]. Higher primary productivity and deposition rates are promoted through the mixing of saline and fresh water. Thus, estuarine and coastal sediments tend to be rich in organic matter [30-32]. This organic matter can provide energy and electron donors for sulfate reduction, intensity of methane flux and other biogeochemical processes [33-35]. Intensity of methane flux and sulfate reduction are the main processes of the biogeochemical cycle in estuarine and coastal sediments and are also the foundation of the sedimentary carbon and sulfur biogeochemical cycles [36-38]. The sediment surface in various environments shows pockmarks with different shapes, sizes and formation mechanisms as a result of the combined action of hydrodynamic forces, sediment transport and shallow subsurface gas flow [39,40]. The biogeochemical processes and sedimentary environments of such pockmarks are areas of increasing interest to researchers [41,42].

The region offshore of Zhejiang and Fujian provinces represents the largest underwater bank slope-type argillaceous deposit in China's coastal zone [43]. Due to its wide distribution range, large deposition thickness, high source diversity, complex hydrodynamic conditions and other factors, this area provides an excellent natural test site for the study of Quaternary environmental evolution [44,45]. Since the late Pleistocene, the Taiwan Strait has been affected by tectonic compression, extension and compression again, along with sea-level fluctuations and the uneven uplift and subsidence of local blocks, resulting in complex submarine topography and a complicated sedimentary environment. Early investigations showed that the methane concentration in the shallow sedimentary environment was relatively high, so it was speculated that there might be abnormal characteristics such as oil and gas source rocks in the underlying strata. In recent years, both the special investigations of Mission 908 and geological support engineering have found a large number of

pockmarks and shallow gas outflow in this area, and they appear in areas with different types of deposits [46]. Although pockmark landforms are common on the seafloor of continental margins globally, little is known about the geochemical characteristics of the sediment, activity status, trigger mechanism and formation time of submarine pockmark landforms, especially shallow-water landforms. Previous research shows that most pockmarks are inactive, but what is the current status of shallow-water pockmarks? Is it possible to obtain some information on the activity of pockmarks through pore water geochemistry? The formation of pockmarks is usually related to the leakage of submarine fluids. Therefore, what are the main biogeochemical reaction rates in sediments and the contributions of active fluids, such as methane and dissolved inorganic carbon, to shallow-water pockmarks? Understanding these processes is also of important to understanding the global carbon cycle. Therefore, in this study, we selected pockmark landforms with different sedimentary environments in the coastal waters of Fujian Province to determine the spatial characteristics of the SMTZ distribution, total organic carbon (TOC) content, dissolved inorganic carbon (DIC) content and δ^{13}C values in pockmark landforms with different morphologies, as well as other important indicators of sedimentary environment types, combined with the characteristics of stratigraphic structure, hydrodynamic conditions and regional material sources. This paper analyzes the genetic mechanism and development process of different forms of pockmark landforms and preliminarily constructs a development model of pockmark landforms in different sedimentary environments.

2. Study area

The offshore area of Fujian (32°33′–27°11′N and 117°10′–120°50′E) in the western Pacific Ocean is adjacent to southeastern China and is bounded by the Taiwan Strait to the east, Zhejiang to the north and Guangdong to the south (Figure 1) [47]. The main sediment sources for coastal accumulation landforms are sediments carried by runoff in mountain streams and rivers. These sediments are transported to the coast by runoff or directly washed into the alongshore current system, and their input affects the erosional and depositional processes of beaches [40,46]. The total watershed area in Fujian is 11.03×10^4 km², and the average annual total amount of outflow water is 10380.54×10^8 m³ (1956–2018). The Minjiang River accounts for 55.4% of the total, the Minnan rivers supply 2910×10^8 m³ (28% of the total) and the

Mindong rivers supply $1720×10^8\,m^3$ (16.4% of the total). The average annual amount of sediment entering the sea in the whole province is $2000×10^4\,t$, and the Minjiang, Jiulongjiang and Jinjiang Rivers account for 50% of the total sediment load.
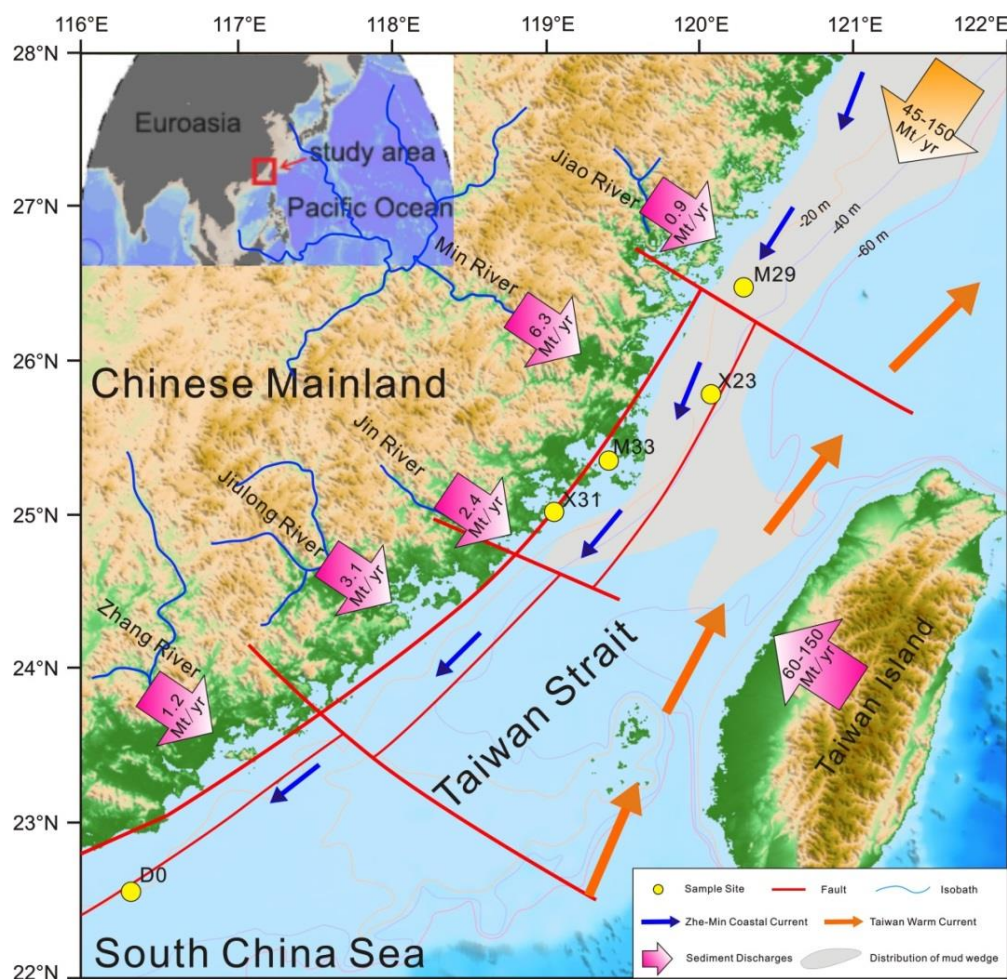

Figure 1. Location map and sampling stations of study area. In this map, isobaths of 20, 40, and 60 m are shown by the thin light-yellow, purple, and red lines, respectively. Black and orange arrows indicate the Zhe-Min Coastal Current and Taiwan Warm Current, respectively [48]. Arrows marked with gradual magenta and numbers indicate fluvial sediment discharge (Mt/yr) from the Chinese mainland [29] and Taiwan. The mud wedge on the inner shelf of the East China Sea was marked with translucent gray areas. Fluvial drainage systems surrounding the TS and location of Cores M29, X23, M33, X31and D0 (Yellow circle).

The coastal geology of Fujian is a part of the western Pacific trench–island arc–marginal sea system and is affected by the action of four plates: Eurasia, India, Pacific and Philippine Sea [49]. The Quaternary neotectonic activity is characterized by the differential uplift of fault blocks and by fault activity, and the main tectonic deformation is the reactivation of NE, NNE, NW and NNW trending faults that

originally formed in the Yanshanian. Based on the linear features generated by the NW-SE- and E-W-trending faults, the intensity of faulting since the late Pleistocene increased seaward from the land to the ocean. The differential activity of the faults and fault blocks has controlled the development of the Quaternary basin, plain and bay. In the coastal areas, the activity of the Changle-Zhaoan fault zone has controlled the distribution of the Quaternary basin and plain in the northeast along with the development of a NE-trending graben and horst system and a bay. The fault activity in the northwest has been greater since the late Pleistocene and has controlled most of the basin development in this area. The offshore area is to the west of a fault in the littoral zone, and intense fault-related subsidence has prevailed in the Taiwan Strait during the Quaternary. Consequently, numerous fractures and vertical conduits have developed in the coastal sediments due to criss-crossing tectonic structures, providing important passages for subsurface gas movement [50,51].

3. Materials and methods

3.1. Field work

3.1.1. Bathymetric measurements

From May 2014 to September 2016, a multibeam echosounder (SeaBeam 3012, L3) was used to investigate the submarine topography of muddy areas offshore of northern Fujian, estuarine areas off central Fujian, sandy areas offshore of southern Fujian and other coastal areas. When the water depth was less than 10 m, the distance between survey lines was set at 50 m. In areas where the water depth was 10–20 m, the distance between survey lines was 100 m, and when water depths were >20 m, the distance between survey lines was 200 m. The distance between the survey lines was changed according to the actual water depth in the survey area, the sweep width of the instrument and sea conditions. An overlap of 10% between adjacent survey amplitudes was ensured, and a total area of 500 km^2 was surveyed with the multibeam echosounder.

3.1.2. Sediment collection

In May 2014 and June 2015, a scientific research cruise on the ship *Runjiang* and *Yanping No. 2* recovered sediment core samples from five locations in the nearshore area of the western Taiwan Strait (Table 1, Figure 1). The five sites are located in the muddy areas off Zhejiang and Fujian (M29 and X23), in Xinghua and Meizhou bays

offshore of central Fujian (M33 and X31) and the sandy area offshore of southern Fujian (D0). The water depths were 15–60 m, and the core lengths were 106–153 cm. Samples from M33 and X31 had high sedimentary water and organic matter contents and an obvious putrid odor and were mainly composed of black-gray clay with plant debris. Samples from M29 and X23 were high in water content, and the organic matter decreased with distance from land; the sediment had a slightly fishy odor and was composed of grayish-green sandy clay containing little biodetritus and plant root residues. Samples from D0 had low water and organic matter contents and were composed of yellowish-green silty sand with little biodetritus. The bottom water temperatures were 26.65–29.64°C, and the salinity was 32.11–33.97.

Table 1. Sampling locations and parameters measured in the field at the five stations

Stations	Langitude	Latitude	Water depth /m	Sample length	Temperature /℃	Salinity	Sediment type
M29	120°20′18″	26°28′10″	26	146	26.65	33.66	Clay
X23	120°08′25″	25°42′40″	38	153	27.07	33.97	Clay
M33	119°25′18″	25°20′18″	16	135	29.17	32.11	Silt
X31	119°00′01″	25°3′59″	19	144	28.33	32.82	Silt
D0	116°10′17″	22°41′59″	22	106	29.64	33.21	Sand

Sediment samples from the five locations were recovered with a gravity pipe sampler (counterweight = 1 ton; length = 4 m; inner diameter = 75 mm). Holes were drilled in the outer wall of the PVC casing at 5 cm intervals (φ = 1 cm) and then sealed with electrical adhesive tape before sampling. The pipe wall was wrapped with a film and sealed with the same adhesive tape. The sediment cores were arranged horizontally on an indoor bearing platform, and 3–5 cm samples were taken and placed into bottles (50 cm^3, Bellco, USA) under anaerobic conditions while inhibiting methanogens added in advance (1 mol/dm^3 NaOH). The bottle openings were sealed with a rubber plug after nitrogen purging, and the bottles were sealed with aluminum caps, labeled and stored cold. The sedimentary headspace methane content and carbon isotopes were measured using these samples. In addition, Macro Rhizon pore water samplers (sampling head of 5 cm) were inserted into the sediment core in the premanufactured holes and were equipped with 5 cm^3 vacuum tubes. Sediment pore water was extracted under negative pressure on site; 2–3 tubes of pore water were collected from each layer, sealed with Parafilm (Sigma-Aldrich), labeled and preserved in cold storage. The cores were cut into 1 m sections upon completion of pore water extraction and preserved in a refrigerated locker (4°C) after being wrapped

and sealed.

3.2. Data processes

3.2.1. Bathymetric data process

The original multibeam data were processed by sound velocity profile corrections, tidal level corrections and parameter corrections; noisy points were eliminated effectively. Finally, a high-precision submarine digital elevation model (grid resolution of 50 m) was established, and the seabed slope and terrain profile were calculated to analyze the relief changes in the study area and to determine the size, shape, distribution and other related parameters of the pockmarks.

3.2.2. Laboratory analysis of sediment samples

The analysis was performed with an Iso prime 100 continuous flow-isotope ratio mass spectrometer (CF-IRMS). For each sample, 0.5 ml of sample was to a glass bottle with a round bottom, high-purity helium was blown over the sample, and 5-6 drops of anhydrous phosphoric acid were added. After reaction at 40 ºC for 4 hours, the produced CO_2 was separated by a chromatographic column and then sent to a mass spectrometer for carbon isotope determination. The analysis accuracy was better than 0.2 ‰. The linear formula relationship between the signal intensity of $^{44}CO_2$ and the DIC contents of 0.85 mmol, 2.07 mmol and 3.93 mmol DIC samples was established to calculate the DIC content. Each sample was measured twice, the experimental error was less than 5%, and the standard deviation was ± 0.2%. The reference standard for carbon isotopes is V-PDB (the reported carbon isotope values are the corrected result based on the international standard V-PDB). The DIC contents and δ^{13}C-DIC values were analyzed on the science and technology sharing experimental platform of the Third Institute of Oceanography, Ministry of Natural Resources.

The pore water was diluted 500 times with ultrapure water. The anions Cl^- and SO_4^{2-} and cations Na^+, K^+, Mg^{2+}, and Ca^{2+} were measured by the Diane company's Dionex ICS-900 ion chromatograph. When analyzing anions, 4.5 mmol Na_2CO_3 and 0.8 mmol $NaHCO_3$ were used as the eluent, 25 mmol H_2SO_4 as the regeneration solution, 50 μl as the injection volume and 1 ml/min as the flow velocity, and the chromatographic column was an ionPAC AS19. Repeated measurements of standard seawater show that the standard deviations of all anions and cations were less than 0.5% [52]. The pore water pH was measured with a CHN 86801 (Orion, USA) pH meter

(accuracy of ±0.001). The ion content of the pore water was analyzed on the science and technology sharing experimental platform of the Third Institute of Oceanography, Ministry of Natural Resources.

The 3 ml of sediment in the weighing bottle was dried at 105 ºC and weighed after achieving a constant weight [53]. The weights of the sample before and after the experiment were then compared. The porosity was presented by the volume of water contained in the sediment per unit volume. The sediment samples were pretreated by removing impurities, grinding and acidification. The sediment samples were pretreated to remove impurities, ground and acidified, after which a Vario EL-III (Elementar, UK) elemental analyzer was used to measure the TOC and total nitrogen (TN) and a Delta Plus II XL isotope mass spectrometer (IR-MS) was used to determine the $\delta^{13}C_{TOC}$. The standard deviation (σ) was ±0.2% (IR-MS). The sediment samples were analyzed at the State Key Laboratory of Marine Geology (Tongji University).

3.2.3. Methane flux calculation

Sedimentary organic matter can affect the diffusion of CH_4; thus, the CH_4 diffusion flux in sediments in the study area was calculated according to Fick's laws (Eqs. 1 and 2):

$$J = -\varphi\, Ds\, \frac{\mathrm{d}c}{\mathrm{d}x}, \text{(Eq. 1)}$$

where J is the diffusion rate [mmol/(m^2·a)], φ is the sediment porosity, Ds is the sediment diffusion coefficient (m^2/a), c is the CH_4 concentration (mmol/dm^3) and x is the sediment depth (m).

$$Ds = \frac{D_0}{1 + n(1-\varphi)}, \text{(Eq. 2)}$$

where $n = 3$ (lithology factor of silty clay) and $D_0 = 1.4 \times 10^{-5}$ cm^2/s (initial diffusion coefficient of methane at 20 ºC).

4. Results

4.1. Morphological features of various pockmarks

According to the multibeam data, several types of pockmarks were identified. The main types included: (1) small pockmarks, which have widths of 1–10 m,

diameters of <5 m, depths of up to 0.5 m, and a wide distribution throughout the study area; (2) circular pockmarks (diameter=5–30 m, depth=1–5 m), which have bowl-like cross-sections (inner slopes of the pockmark are gentle) or asymmetric cross-sections (inner slopes are steep), and single pockmarks are widely distributed around these more normal pockmarks; (3) elongated pockmarks (depth=1–8 m), which have one much longer axis, and this type often appear on slopes or areas affected by strong bottom water flow and is mainly distributed in the northern muddy areas; (4) chain-type pockmarks, which are small pockmarks or small normal pockmarks arranged in a line or curved shape and have lengths that can extend for thousands of meters because they are generally formed from concentrated fluid leakage along approximately vertical fault or weak zones, and this type is mainly found in estuaries and bays; and (5) compound pockmarks, which are normal pockmarks appearing in groups or formed through the combination of several pockmarks, and this type is mainly distributed in the southern sandy area (Table 2).

Table 2. Distribution and types of pockmarks in study area

NO.	Area	Types	Characteristics	Sedimentary type
1	Zhe-Min muddy	Unit, circular, liner	Medium to small diameter, depth does not exceed tens of meters, linear distribution, the overall size is not large.	Silty clay
2	Bay mouth	Unit, circular, elongated	Medium to small diameter, depth of not more than a few meters, shape asymmetry, the overall size is small or medium.	Clayey silty
3	Sandy	Circular, elongated, mixed	The diameter is medium to large, the depth is not more than ten meters, the form is asymmetrical, into groups appear, the scale is large.	Silty sand

4.2. Geochemical features of pore water in the sediment

4.2.1. SO_4^{2-} and CH_4 concentrations in pore water

The SO_4^{2-} and CH_4 concentrations in sediment pore water from five stations (M29, X23, M33, X31 and D0) are shown in Figure 2. The CH_4 concentrations in pore water gradually increased with sediment depth, while SO_4^{2-} concentrations gradually decreased. The SO_4^{2-} concentrations in the surface sediment pore water were higher, and the SO_4^{2-} concentration profiles showed a linear decrease with depth; the correlation coefficient r was 0.83 (M29), 0.92 (X23), 0.75 (M33), 0.71 (X31) and 0.55 (D0) until the SO_4^{2-} was consumed completely. The corresponding sediment

depths where the pore water SO_4^{2-} was consumed completely were 65 cm (M29), 55 cm (X23), 95 cm (M33), 110 cm (X31) and 200 cm (D0); these depths correspond to the SMTZ. The surface sediments at station D0 were silty sediments containing incompletely decomposed humus. Consequently, the microbial degradation was not complete, and the content of active organic matter was low. Thus, the geochemical activity in the surface sediment pore water at D0 was not obvious, and the SO_4^{2-} concentration was low in the surface layer.
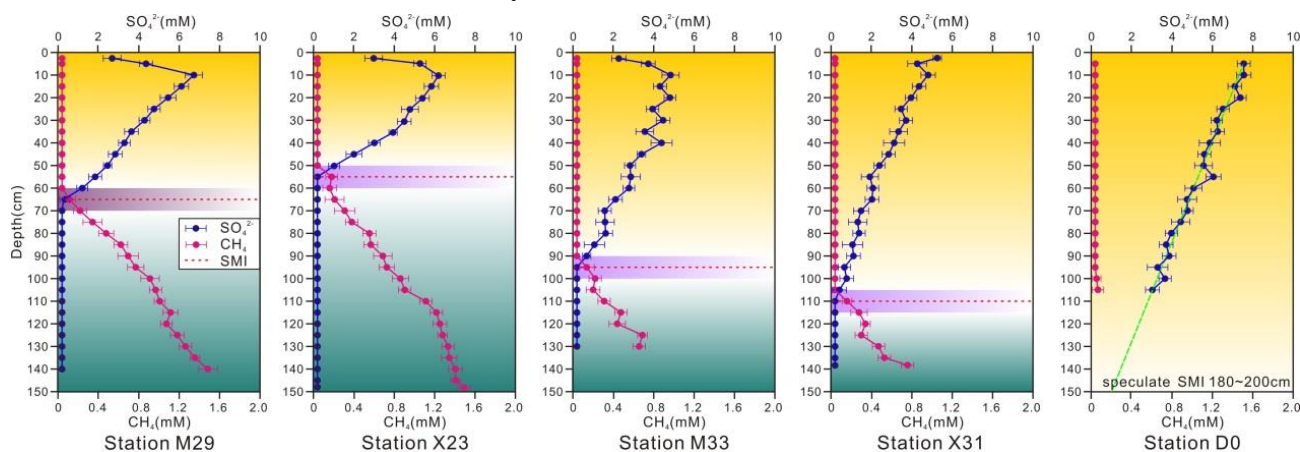
Figure 2. Concentrations profile of sulfate and methane in pore water.

The changes in pore water CH_4 and SO_4^{2-} concentrations were obviously different. The CH_4 concentrations in the pore water were relatively low in the upper sedimentary layers and exhibited only slight variations, but the CH_4 concentrations sharply increased in the vicinity of the SMTZ. The CH_4 concentrations rapidly increased from 25.60 μmol/dm^3 to 1567.15 μmol/dm^3 at 140 cm at M29, 37.55 μmol/dm^3 to 1575.32 μmol/dm^3 at 150 cm at X23, 30.58 μmol/dm^3 to 699.67 μmol/dm^3 by 125 cm at M33, and 40.98 μmol/dm^3 to 782.42 μmol/dm^3 at 140 cm at X31. However, limited CH_4 was found at D0, with only a minor concentration at 100 cm.

4.2.2. DIC concentrations and $\delta^{13}C_{DIC}$ in pore water

The DIC concentrations and $\delta^{13}C_{DIC}$ values of the sediment pore water are shown in Figures 3, respectively. The DIC concentrations of the sediment pore water gradually increased with depth at all sites until the maximum values were reached in the vicinity of the SMTZ. The concentrations then decreased and generally remained stable; however, the pore water DIC increased again at the bottom of some stations. At M29, the pore water DIC in the surface sediment was 6.25 mmol/dm^3, increased to 12.08 mmol/dm^3 at 60 cm, and then gradually decreased with depth until 120 cm,

below which it remained stable. At X23, the DIC increased from 4.02 mmol/dm^3 to 16.24 mmol/dm^3 at 55 cm and then gradually decreased with depth, but a second concentration peak (11.89 mmol/dm^3) was present at 110 cm. At M33, the surface sedimentary DIC in pore water was 6.11 mmol/dm^3, increased to 10.42 mol/dm^3 at 100 cm and gradually decreased with depth to a stable value at 120 cm. At Y31, the DIC increased from 3.74 mmol/dm^3 to 8.16 mmol/dm^3 at 115 cm and then gradually decreased with depth to a stable value. At D0, the DIC gradually decreased to 16.25 mmol/dm^3 from 0 to 105 cm.
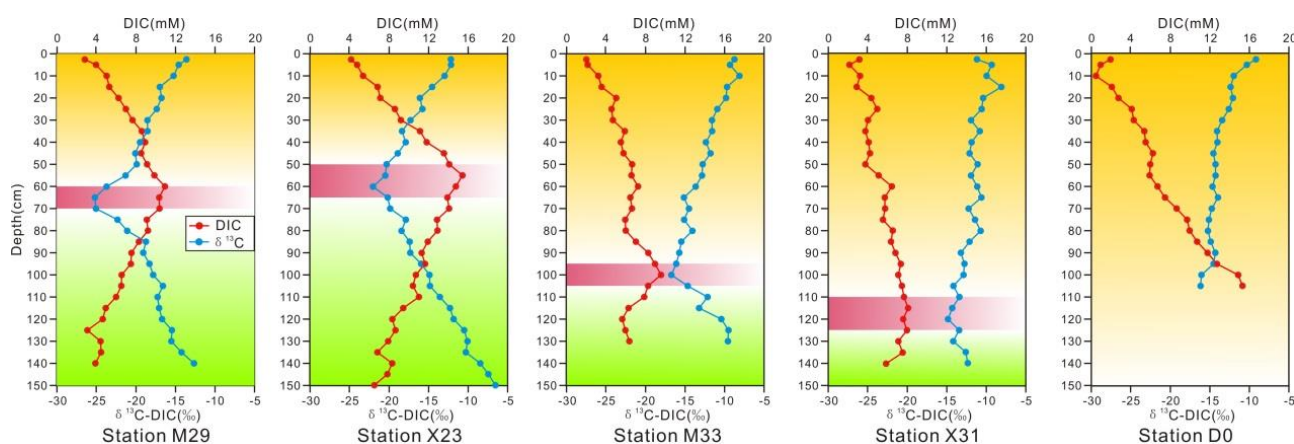

Figure 3. Concentrations profile of DIC and $\delta^{13}C_{DIC}$ in pore water.

The sedimentary pore water $\delta^{13}C_{DIC}$ values all showed rightward convex curves with peak negative carbon isotope values of -25.43‰ (M29), -22.91‰ (X23), -17.75‰ (M33), -15.02‰ (X31) and -15.98‰ (D0) at 65 cm (M29), 60 cm (X23), 100 cm (M33), 120 cm (X31) and 105 cm (D0) below the sediment surface. The most negative $\delta^{13}C_{DIC}$ values were close to the SMTZ at all analyzed stations, except for KC1. In general, the $\delta^{13}C_{DIC}$ values decreased with increasing depth to the SMTZ, below which they increased.

The vertical changes in sedimentary TOC are shown in Figure 4. The apparent trends include the following: (1) the surface sedimentary TOC gradually decreased from north to south, with average contents of 1.78% (X23) >1.54% (M29) >1.22% (M33) >1.09% (X31) >0.74% (D0), and (2) the sedimentary TOC gradually decreased with increasing depth. The TOC content is affected by the input of detrital terrigenous material. There is an obvious change in sedimentary TOC with depth at M29, but at sites farther south, there were smaller TOC changes from the sediment surface to the bottom of the column.
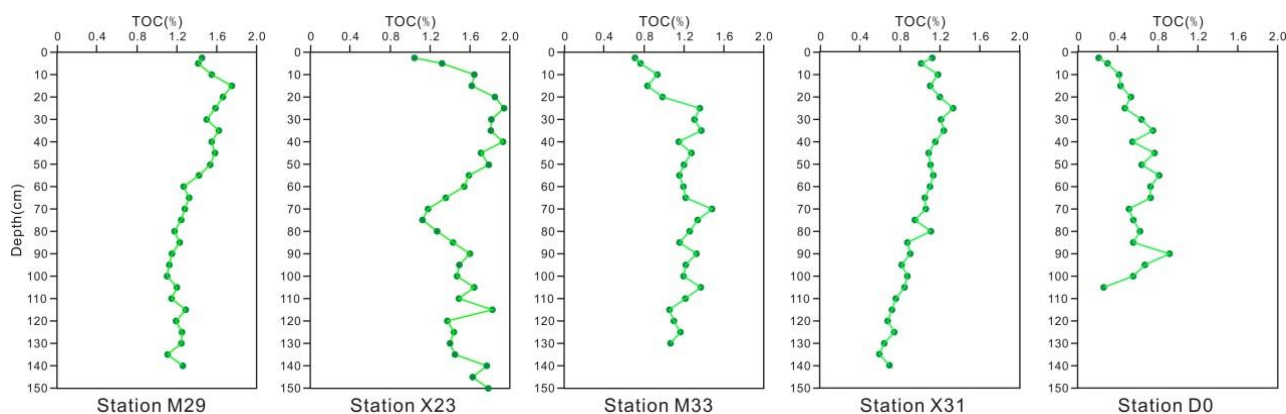
Figure 4. Components profile of TOC in sediments.

4.2.3. Methane flux

Sedimentary organic matter can affect the diffusion of CH_4. Thus, the CH_4 diffusion flux in the sediments of the study area was calculated according to Fick's laws (Eqs. 1 and 2). The methane diffusion fluxes of the five stations, including M29, X23, M33, X31 and D0, were 15.17×10^{-2} mmol•m^{-2}•a^{-1}, 18.85×10^{-2} mmol•m^{-2}•a^{-1}, 9.31×10^{-2} mmol•m^{-2}•a^{-1}, 8.72×10^{-2} mmol•m^{-2}•a^{-1}, 2.89×10^{-2} mmol•m^{-2}•a^{-1}, respectively, with an average value of 10.99×10^{-2} mmol•m^{-2}•a^{-1} (Table 3). In combination with Figure 5, the TOC content distribution in sediments indicates that the input of organic matter in sediments is a key factor controlling the methane diffusion flux at the bottom. With an increase in the upward methane diffusion flux, the consumption of methane and sulfate, namely, the occurrence of the intensity of methane flux process, is intensified and causes the upward migration of the SMTZ in the sediment.

Table 3. Sediment diffusion coefficients *DS*, calculated diffusive intensity of methane flux and the average content of TOC in surface sediments

Station	Porosity	Ds(m^2 • a^{-1})	J(mmol·m^{-2} • a^{-1})	TOC(%)
M29	0.65	2.53×10^{-2}	15.17×10^{-2}	1.54
X23	0.71	2.75×10^{-2}	18.85×10^{-2}	1.78
M33	0.80	3.29×10^{-2}	9.31×10^{-2}	1.22
X31	0.76	2.65×10^{-2}	8.72×10^{-2}	1.09
D0	0.85	4.04×10^{-2}	2.89×10^{-2}	0.74
Average	0.76	3.05×10^{-2}	10.99×10^{-2}	1.27

5. Discussion

5.1. The formation mechanism of pockmarks

Pockmarks are crater-like depressions that appear in fine-grained sediments on

the seafloor. They have received considerable attention because they can provide important information on fluid activities in continental margins [3]. Paul et al (2008) believed that free gas first accumulates under fine-grained sediments with sealed capillaries [54]. As the amount of free gas increases, the gas buoyancy eventually exceeds the capillary pressure, and the free gas pierces the sealing layer and migrates into the overlying sedimentary layers, forming upward-flowing gas that entrains pore water as it discharges from the sediment. Due to the upward flow of gas and pore water, the surface sediments of the seabed are deformed, and the liquefied sediments are transported by the fluid flow, forming pockmarks. Consequently, fluids play an important role in the formation of pockmarks.

Because the seafloor stratigraphy and geomorphology are complex and changeable, pockmarks are affected by many factors after formation, such as continuous fluid leakage, bottom currents, tectonic activity and sedimentation, with the result that the diameter, depth and plan-view configuration of pockmarks can vary [10,55]. Weber et al (2002) proposed that the ratio of the slope and diameter of the inner wall to the depth of a pockmark reflects different development stages. The depth of newly generated or recently active pockmarks is deeper, and the inner walls are steeper, whereas pockmarks with larger diameters and shallower depths are older, as the bottoms have been infilled to some degree with sediment [56]. It can be seen from Figure 5 that most of the pockmarks in the study area are located in the offshore shallow sea area. Due to the thin sedimentary cover, strong hydrodynamic forces, medium- and small-scale pockmarks, the depth and diameter of pockmarks are not more than 10 m. These pockmarks are mainly round pockmarks with shallow depths (1-2 m) and elongated pockmarks with greater depths (3-6 m). The boundary between individual pockmarks in the coarse particle sedimentary area is not obvious because of the strong hydrodynamic alteration following their formation.
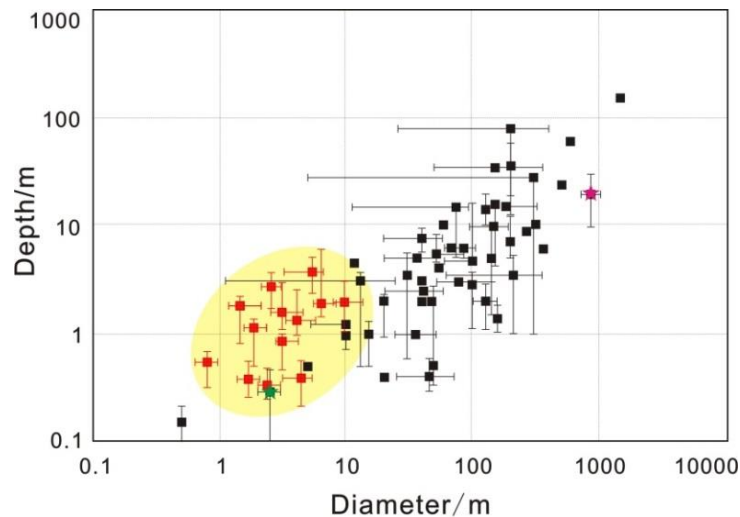
Figure 5. The relation diagram of pockmark diameter and depth. The line segment represents the variation range of the size of a single pockmark, and the point represents the size of a single pockmark area or the average value of the size of a single pockmark.

Hinrichs (1999) suggested that the formation of small pockmarks (with diameters <5 m) is related to the slow leakage of pore water, while the formation of more common pockmarks may be closely related to periodic or intermittent gas eruptions from the seabed [57]. Free gas in deeper strata can accumulate in shallow strata as bubbles with pore water filling the space between bubbles. With continuous gas accumulation, the pressure gradually increases until the storage strata rupture; the gas then erupts from the seabed along a fracture and forms pockmarks. Small pockmarks are mostly distributed along underwater slopes and plains of estuaries and coasts at water depths of 5–100 m. In these areas, the terrigenous input is abundant, and structural activity is common, which favors organic matter decomposition and gas accumulation in the sediments and the formation of pockmarks of different sizes on the seafloor [58-60]. As seen from Figure 6 and Figure 7, the pockmarks in the estuary area (Figure 5, green asterisk) [8] feature shallow water depths, small scales and shallow SMTZs. The pockmarks in the submarine slope area (Figure 5, pink asterisk) [10] feature greater water depths, larger scales, and deep to nonexistent SMTZs. The pockmarks in the study area are present in a shallow-water area, and the depths and scales of the pits are small. Affected by the sedimentary environment and hydrodynamic conditions, the morphologies and scales of the pockmarks are quite different.
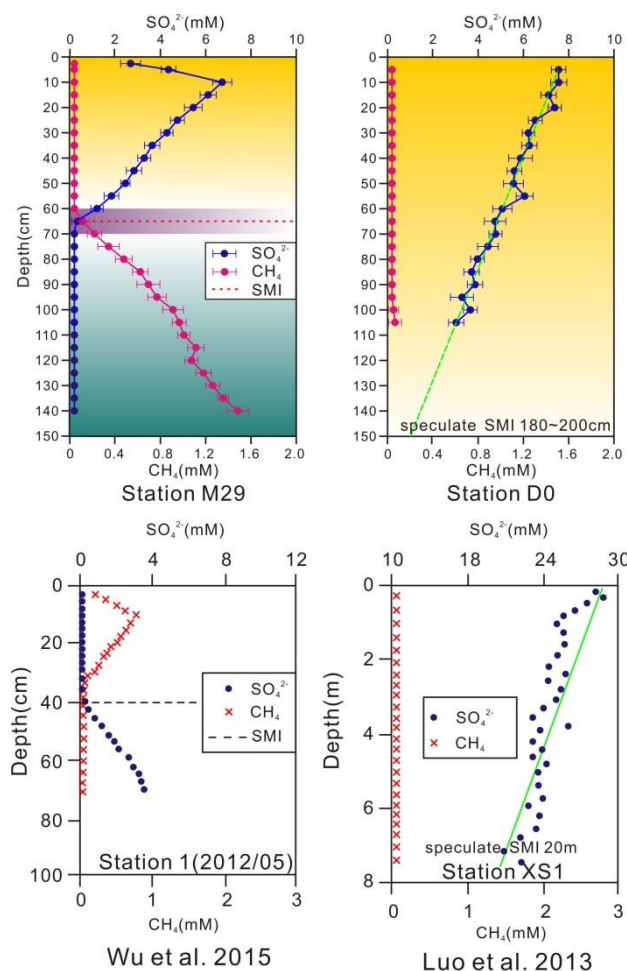
Figure 6. Depth comparison diagram of sulfate and methane transitional zone

The results of physicochemical property and isotopic composition analysis of the shallow surface sediments associated with typical pockmark morphologies showed that 1) along the northern coast of Fujian, there is almost no input of terrestrially sourced materials from large rivers, the C/N ratio is indicative of a marine facies, and marine biogas is the main component based on the carbon isotopic composition. In the argillaceous zone, active materials are less abundant, and the sulfate content has a tendency to decrease, but this trend is not obvious. (2) Outside the mouth of the Minjiang River, in the underwater delta of the estuary, the substrate consists of sand and mud, the C/N ratio shows indicates the input of terrestrially sourced substances, active substances are relatively abundant, the reduction of sulfate is strong, the SMTZ is relatively shallow, and the carbon isotopic composition suggests that biogenic gas is common. (3) In the submarine depression offshore of southern Fujian Province (off Dongshan Peninsula), the carbon isotopic composition of the sandy bottom material shows that the organic matter is of mixed origin, originating from both the sea and

land, the biogenic gas of mixed pyrolysis is derived from less active material (indicating that the underlying formation contains oil, gas and methane), the sulfate reduction is strong, and the SMTZ is shallow.

5.2. Intensity of methane flux in various sediment environments

The shapes and scales of various pockmarks are directly correlated with the sedimentary environment [59]. When the sediments feature a reducing environment, organic matter is oxidized by sulfate-reducing bacteria using pore water SO_4^{2-} as an oxidizing agent in the reaction $2CH_2O+SO_4^{2-}\rightarrow 2HCO_3^-+H_2S$. Consequently, pore water SO_4^{2-} concentrations decrease. Near the SMTZ, SO_4^{2-} and CH_4 participate in intensity of methane flux in the reaction $CH_4+SO_4^{2-}\rightarrow HCO_3^-+HS^-+H_2O$; thus, sedimentary DIC mainly exists as HCO_3^-. As a result, pore water pH increases, equilibrium shifts to the right in the reaction, and SO_4^{2-} also decreases with depth. With increasing CH_4 concentrations, intensity of methane flux equilibrium moves to the right in the reaction equations, and SO_4^{2-} decreases [61,62]. Borowski (1999) identified strong intensity of methane flux in the upper stratum of a thick Quaternary sedimentary sequence on Blake Ridge [63], which explained the shallow SMTZ and rapid decrease in SO_4^{2-} in the pore water profiles (Table 4). Thus, the depth of the SMTZ can indicate the strength of intensity of methane flux in the sedimentary environment. The average SMTZ depth in the study area was approximately 180 cm. The SMTZ is shallower in the estuary than in other coastal areas because of the stronger intensity of methane flux.

Table 4. Compared SMTZ depth of pockmarks in study area with other areas

Area	Water depth/m	SMI depth/cm
This study	16~38	50~200
Shenhu sea area	800~1 500	200~1 750
Baiyun depression	1 000~1 200	600~1 100
Saanick bay	225	10~20
Skan bay	10~65	20~30
Black sea	130~180	200
Continental margin of Chile	800~2 700	220~400
Carolin ridge and Blake submarine plateau	1 300~4 750	1 300~6 000

In the early diagenetic process of marine shallow sediments, sulfate reduction is mediated by sulfate-reducing bacteria, which oxidize organic carbon, resulting in a change in the sulfate concentration gradient. Therefore, the oxidation of organic matter is the main reason for the change in sulfate concentration. In shallow marine

sediments, intensity of methane flux generally occurs in one sedimentary zone, and the upper transitional zone of this zone is known as the SMTZ [17,64]. The CH_4 generation zone is below the SMTZ. CH_4 is generated by reduction reactions between in situ microorganisms and CO_2 ($CO_2+4H_2 \rightarrow CH_4+2H_2O$) and acetate fermentation ($CH_3COOH \rightarrow CH_4+CO_2$). CH_4 can also be generated through the decomposition of oil and natural gas hydrates [65,66]. The analysis of CH_4 offshore of Fujian showed that concentrations in shallow sediments from the estuaries increased with depth. Because the electron uptake capability of sulfate-reducing bacteria is relatively high, the activity of methanogenic bacteria is restricted; once most SO_4^{2-} is reduced (more than 80%), CH_4 generation starts. Conditions that encourage a shallow SMTZ include a high deposition rate, rapid sedimentary burial and a high organic matter content. These conditions result in a strong reducing environment and increases the generation of CH_4, which produces a high intensity of methane flux (Table 3). Thus, intensity of methane flux during diagenesis, particularly in the early stages of sedimentary burial, is closely related to the sediment deposition rate, organic matter content, porosity and redox potential [67,68].

The methane concentration increases gradually below the SMTZ. The DIC produced by intensity of methane flux inherits the relatively light carbon isotopic composition of methane, while the DIC produced by organic matter oxidation has a relatively heavy carbon isotopic composition. The diffusion coefficient of $^{12}CH_4$ is greater than that of $^{13}CH_4$ because of isotopic effects during diffusion, and $^{12}CH_4$ is oxidized first during intensity of methane flux, increasing the $^{12}CH_4$ concentration gradient. As a result, the diffusion of $^{12}CH_4$ into upper sediment layers increases. The amount of organic matter entering the deep CH_4 zone increases as the organic matter content of the surface sediments increases, and the CH_4 concentration and diffusion flux in sediment pore waters increases. The joint consumption of CH_4 and SO_4^{2-} during intensity of methane flux increases as the upward-diffusing intensity of methane flux increases and causes the SMTZ to shift into a shallower position in the sediment column [69,70]. As seen from Figure 4, the δ^{13}C-DIC values of pore water at stations M29, X23 and M33 tend to decrease first and then increase with the change in depth, which is consistent with the change trend of the sulfate group and reaches the lowest value near SMTZ, indicating that intensity of methane flux has a strong effect. Although the high contents of organic carbon at stations X31 and D0 will also consume sulfate in pore water, there is no corresponding decrease in the organic

carbon content of the layers with the sharp decrease in the sulfate content in the sediments at these stations, indicating that the consumption of sulfate by organic carbon is not the main factor responsible for the sharp decline in the sulfate ions in pore water.

5.3. Development stages of pockmarks and application of this information

The shape, size and scale of pockmarks are directly related to the type of bottom material and the gas production flux of the underlying strata. Different sedimentary environments and hydrodynamic conditions produce different shapes, sizes and scales of pockmarks, which indicate different development stages and different types of sedimentary environments. In the initial stage of pockmark formation, the pockmarks are mostly round or elliptic and are then subsequently affected by seabed collapse or bottom currents, forming various shapes, such as elongated and crescent shapes. Long-term fluid leakage is not a necessary condition for maintaining pockmark morphology [71,72]. Other mechanisms can also maintain and transform pockmark morphology. For example, a weak bottom current near the sea floor forms upwelling in pockmarks, which can prevent sediments from accumulating in pockmarks and thus maintain the original pockmark morphology [7,73].

Therefore, according to the shape, scale, substrate type, gas flux and hydrodynamic conditions of the underlying strata in the study area, the following stages of pockmark geomorphology in the study area were identified. (1) In the initial stage of pockmark formation, individual pockmarks are usually round or oval in shape (Figure. 7-I), and the distribution of pockmarks is relatively independent. intensity of methane flux plays a strong role in the sedimentary layer, fluid actively escapes the seabed, and multiple pockmarks can develop in lines, forming chain pockmarks. Such pockmarks are easily formed in the southern part of the Zhejiang and Fujian mud area. (2) Due to erosion by tidal currents and weak hydrodynamic forces, the pockmarks at the mouth of the bay are obviously elongated along the flow direction. The inner walls of the pockmarks gradually disappear over time due to erosion. The intensity of methane flux effect weakens (Figure. 7-II), and circular and chain pockmarks gradually develop into elongated pockmarks. (3) For pockmarks developed in coarse sediments, due to the weak role of intensity of methane flux (Figure. 7-III), the pockmarks that form in the initial stage are subjected to long-term complex hydrodynamic erosion and become integrated, resulting in the formation of complex pockmark morphologies with unclear types. Figure 8 shows the morphologic

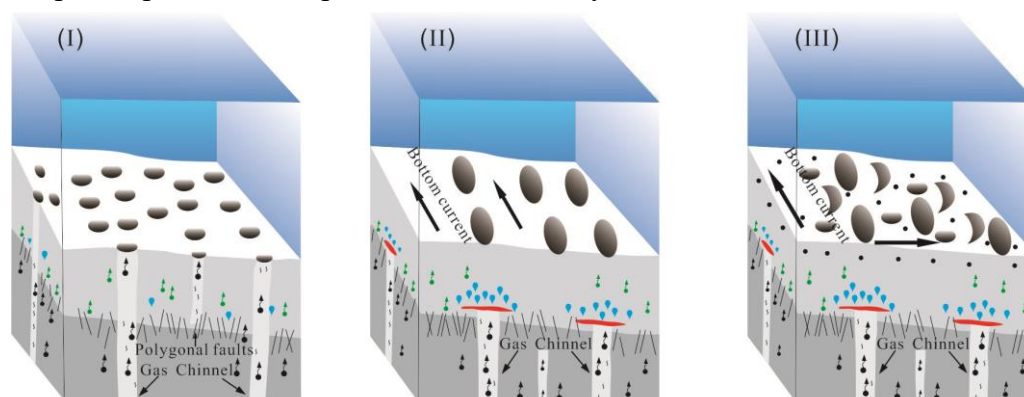development pattern of the pockmark in the study area.

Figure 7. Pattern diagram of development stage and sedimentary environment of pockmark. (I) primary stage by strong intensity of methane flux. (II) growth stage by One-way flow. (III) decline stage by complex dynamic and weak intensity of methane flux.

6. Conclusions

The vertical profiles of pore water CH_4, SO_4^{2-}, DIC and $\delta^{13}C_{DIC}$ values in areas offshore of Fujian Province showed that shallow SMTZs were the result of strong intensity of methane flux activity in the study area. The pore water SO_4^{2-} concentrations showed a linear decrease from the surface until the SO_4^{2-} was almost completely consumed near the SMTZ. At this depth, CH_4 concentrations increased quickly, and the pore water DIC concentrations were obviously higher. The SMTZ depths at M29, X23, M33, X31 and D0 were 60, 55, 95, 110 and 200 cm, respectively.

The sedimentary organic matter and water (porosity) contents, along with microbial activity, affected intensity of methane flux activity in the study area. Because the ^{12}C oxidation rate is higher than ^{13}C and $^{12}CH_4$ is heavier than $^{13}CH_4$, the $\delta^{13}C_{DIC}$ values become slightly more negative. Pore water SO_4^{2-} was consumed through remineralization of organic matter, which increased the upward-diffusing CH_4 in intensity of methane flux reaction zones; thus, the rate of consumed SO_4^{2-} also increased correspondingly and shifted the SMTZ to a shallower depth. In addition, the sediment water content was high, and the active organic matter content increased; a portion of this organic matter was decomposed and consumed through mineralization, and consequently, the quantity of the active organic matter at the bottom of the sulfate reduction zone decreased. The SO_4^{2-} in this zone reacted with CH_4 and was consumed, which promoted intensity of methane flux.

The various development phases of pockmarks are characterized by different

shapes, scales, and intensity of methane flux intensities, which are in turn strongly correlated with different sedimentary environments. The single round pockmarks in the primary phase are normally associated with strong intensity of methane flux. In contrast, elongated pockmarks are associated with weakened intensity of methane flux and usually form under the control of stable bottom current flow, resulting in continuous erosion. Furthermore, compound pockmarks are characterized by very weak intensity of methane flux and represent a relatively long-term adjustment to complicated hydrodynamic conditions.

Conflicts of Interest: The authors declare no conflict of interest.

References

1. King, L.H.; MacLean, B. Pockmarks on the Scotian Shelf. *Geol. Soc. Am. Bull.* **1970**, *81*, 3141-3148.

2. Hovland, M.; Talbot, M. R.; Vales, H.; Qvale, H.; Olaussen, S.; Aasberg, L. Methane-related carbonate cements in pockmarks of the North Sea. *J. Sediment. Res.* **1987**, *57*, 881-892.

3. Hovland, M.; Svensen, H.; Forsberg, C.F.; Johansen, H.; Fichler, C.; Fossa, J.H.; Jonsson, R.;

Rueslatten, H. Complex pockmarks with carbonate-ridges off mid-Norway: products of sediment degassing. *Marine Geology*, **2005**, *218(1-4)*, 191-206.

4. Andresen, K.J.; Huuse, M.; Clausen, O.R. Morphology and distribution of Oligocene and Miocene pockmarks in the Danish North Sea-implications for bottom current activity and fluid migration. *Basin Res.* **2008**, *20(3)*, 445-466.

5. Judd, A.G.; Hovland, M.S. Seabed Fluid Flow-The Impact on Geology, Biology and the Marine Environment. Cambridge: *Cambridge University Press*. **2007**, 50-52.

6. Andrews, B.D.; Brothers, L.L.; Barnhardt, W.A. Automated feature extraction and spatial organization of seafloor pockmarks, Belfast Bay, Maine, USA. *Geomorphology*. **2010**, *124(1/2)*, 55-64.

7. Brothers, L.; Kelley, J.; Belknap, D.; Barnhardt, W.; Andrews, B.; Maynard, M. More than a century of bathymetric observations and present-day shallow sediment characterization in Belfast Bay, Maine. USA: implications for pockmark field longevity. *Geo-Mar. Lett.* **2011**, *31(4)*, 237-248.

8. Wu, Z.J.; Zhou, H.; Ren, D.; Gao, H.; Li, J. Processes controlling the seasonal and spatial variations in sulfate profiles in the pore water of the sediments surrounding Qi'ao Island, Pearl River Estuary, Southern China. *Cont. Shelf Res.* **2015**, *98(3)*, 26-35.

9. Luo, M.; Wu, L. S.; Chen, D. F. Research status and progress of seabed pockmarks. *Mar. Geol. Fron.* **2012**, *28(05)*, 33-42.

10. Luo, M.; Chen, L.Y.; Wang, S.H.; Yan, W.; Wang, H.B.; Chen, D.F. Pockmark activity inferred from pore water geochemistry in shallow sediments of the pockmark field in southwestern Xisha Uplift, northwestern South China Sea. *Mar. Pet. Geol.* **2013**, *48,* 247-259.

11. Aller, R.C.; Blair, N.E. Early diagenetic remineralization of sedimentary organic C in the Gulf of Papua deltaic complex (Papua New Guinea): Net loss of terrestrial C and diagenetic fractionation of C isotope. *Geochim.Cosmochim.Acta*. **2004**, *68(8)*, 1815-1825.

12. Aller, R.C.; Madrid, V.; Chistoserdov, A.; Aller, J.Y.; Heilbruna, C. Unsteady diagenetic processes and sulfur biogeochemistry in tropical deltaic muds: Implications for oceanic isotope cycles and the sedimentary record. *Geochim.Cosmochim.Acta.* **2010**, *74(16)*: 4671-4692.

13. Chanton, J.P.; Martens, C.S.; Paull, C.K. Control of pore-water chemistry at the base of the Florida escarpment by processes within the platform. *Nature*. **1991**, *349(6306)*, 229-231.

14. Jørgensen, B.B.; Weber, A.; Zopfi, J. Sulfate reduction and anaerobic methane oxidation in Black Sea Sediments. *Deep-Sea Res. Part I-Oceanogr. Res. Pap.* **2001**, *48(9)*, 2097-2120.

15. Jørgensen, B.B.; Böttcher, M.E.; Lüschen, H.; Neretin, L.N.; Volkov, I.I. Anaerobic methane oxidation and a deep H_2S sink generate isotopically heavy sulfides in Black Sea sediments. *Geochim. Cosmochim. Acta*, **2004**, *68(9)*, 2095-2118.

16. Boetius, A.; Ravenschlag, K.; Schubert, C.J.; Rickert, D.; Widdel, F.; Gieseke, A.; Amann, R.; Jørgensen, B.B.; Witte, U.; Pfannkuche, O. A marine microbial consortium apparently mediating anaerobic oxidation of methane. *Nature*. **2000**, *407(6804),* 623-626.

17. Moore, T.S.; Murray, R.W.; Kurtz, A.C., Schrag, D.P. Anaerobic methane oxidation and the formation of dolomite. *Earth Planet. Sci. Lett.* **2004**, *229(1-2)*, 141-154.

18. Niewöhner, C.; Hensen, C.; Kasten, S.; Zable, M.; Schulz, H.D. Deep sulfate reduction completely mediated by anaerobic methane oxidation in sediments of the upwelling area off Namibia. *Geochim. Cosmochim. Acta.* **1998**, *62(3)*, 455-464.

19. Ogrinc, N.; Lojen, S.; Faganeli, J. A mass balance of carbon stable isotopes in an organic-rich methane producing lacustrine sediment (Lake Bled, Solvenia). *Glob. Planet. Change.* **2002**, *33(1)*, 57-72.

20. Ussler, III.W.; Paull, C.K. Rates of anaerobic oxidation of methane and authigenic carbonate mineralization in methane-rich deep-sea sediments inferred from models and geochemical profiles. *Earth Planet. Sci. Lett.* **2008**, *266(3-4)*, 271-287.

21. Böttcher, M.E.; Oelschläger. B.; Höpner, T.; Brumsack, H.J.; Rullkötter, J. Sulfate reduction related to the early diagenetic degradation of organic matter and "black spot" formation in tidal sand flats of the German Wadden Sea (southern North Sea): Stable isotope (^{13}C, ^{34}S, ^{18}O) and other geochemical results. *Org. Geochem*. **1998**, *29(5)*, 1517-1530.

22. Cao, C.; Lei, H.Y. Geochemical characteristics of pore water in shallow sediments from north continental slope of South China Sea and their significance for natural gas hydrate occurrence. *Procedia Environ. Sci.* **2012,** *12(2)*, 1017-1023.

23. Whiticar, M.J. Carbon and hydrogen isotope systematics of bacterial formation and oxidation of methane. *Chem. Geol.* **1999**, *161(1-3)*, 291-314.

24. Hu, Y.; Feng, D.; Liang, Q.Y.; Xia, Z.; Chen, L.Y.; Chen, D.F. Impact of anaerobic oxidation of methane on the geochemical cycle of redox-sensitive elements at cold-seep sites of the northern South China Sea. *Deep-Sea Res. Part II-Top. Stud. Oceanogr.* **2015**, *122*, 84-94.

25. Antler, G.; Turchyn, A.W.; Herut, B.; Davies, A.; Rennie, V.C.F.; Sivan, O. Sulfur and oxygen isotope tracing of sulfate driven methane oxidation in estuarine sediments. *Estuar. Coast. Shelf Sci.* **2014**, *142(4)*, 4-11.

26. Chen, Y.F.; Ussler, III.W.; Haflidason, H.; Lepland, A.; Rise, L.; Hovland, M.; Hjelstuen, B.O. Sources of methane inferred from pore-water $\delta^{13}C$ of dissolved inorganic carbon in

Pockmark G11, offshore Mid-Norway. *Chem.Geol.* **2010**, *275(3-4)*, 127-138.

27. Lei, H.Y.; Cao, C.; Ou, W.J.; Gong, C.J.; Shi, C.X. Oxygen isotope characteristics of foraminiferan from the northern South China Sea sediments and their significance to late Quaternary hydrate decomposition. *J. Cent. South Univ.* **2012**, *19(6)*, 1728-1740.

28. Fossing, H.; Jørgensen, B.B. Measurement of bacterial sulfate reduction in sediments-evaluation of a single step chromium reduction method. *Biogeochemistry*, **1989**, *8(3)*, 205-222.

29. Milliman, J.; Farnsworth, K. River Discharge to the coastal ocean: A global synthesis. *Cambridge University Press, Cambridge.* **2011**, 2-163.

30. Peiffer, S.; Behrends, T.; Hellige, K.; Larese-Casanova, P.; Wan, M.; Pollok, K. Pyrite formation and mineral transitional zone pathways upon sulfidation of ferric hydroxides depend on mineral type and sulfide concentration. *Chem. Geol.* **2015**, *400(2)*, 44-55.

31. Reeburgh, W.S. Anaerobic methane oxidation: Rate depth distributions in Skan Bay sediments. *Earth Planet. Sci. Lett.* **1980**, *47(3)*, 345-352.

32. Freese, E.; Köster, J.; Rullkötter, J. Origin and composition of organic matter in tidal flat sediments from the German Wadden Sea. *Org. Geochem.* **2008**, *39(7)*: 820-829.

33. Wijsman, J.W.M.; Middelburg, J.J.; Heip, C.H.R. Reactive iron in Black Sea sediments: implications for iron cycling. *Mar. Geol.* **2001**, *172(3-4)*, 167-180.

34. Treude, T.; Krüger, M.; Boetius, A.; Jørgensen, B.B. Environmental control on anaerobic oxidation of methane in the gassy sediments of Eckernföorde Bay (German Baltic). *Limnol. Oceanogr.* **2005**, *50(6)*, 1771-1786.

35. Diaz, R.; Moreira, M.; Mendoza, U.; Machado, W.; Böttcher, M.E.; Santos, H.; Belém, A.; Capilla, R.; Escher, P.; Albuquerque, A.L. Early diagenesis of sulfur in a tropical upwelling system, Cabo Frio, southeastern Brazil. *Geology*. **2012**, *40(10)*, 879-882.

36. Allison, M.A.; Nittrouer, C.A.; Kineke, G.C. Seasonal sediment storage on mudflats adjacent to the Amazon River. *Mar. Geol.* **1995**, *125(3-4)*, 303-328.

37. Malinverno, A.; Pohlman, J.W. Modeling sulfate reduction in methane hydrate-bearing continental margin sediments: Does a sulfate-methane transition require anaerobic oxidation of methane? *Geochem. Geophys. Geosyst.* **2011**, *12(7)*, 1-18.

38. Sawicka, J.E.; Jørgensen, B.B.; Bruchert, V. Temperature charcteristics of bacterial sulfate reduction in continental shelf and slope sediments. *Biogeosciences.* **2012**, *9(1)*, 673-700.

39. Schippers, A.; Jørgensen, B.B. Oxidation of pyrite and iron sulfide by manganese dioxide in marine sediments. *Geochim. Cosmochim. Acta*, **2001**, *65(6)*, 915-922.

40. Zhang, L.; Yin, K.; Wang, L.; Chen, F.; Zhang, D.; Yang, Y. The sources and accumulation

rate of Sedimentary organic matter in the Pearl River Estuary and adjacent coastal area, Southern China. *Estuar. Coast. Shelf Sci.* **2009**, *85(2)*, 190-196.

41. Chen, D.F.; Huang, Y.Y.; Yuan, X.L.; Lawrence, M.; Cathles, III. Seep carbonates and preserved methane oxidizing archaea and sulfate reducing bacteria fossils suggest recent gas venting on the seafloor in the Northeastern South China Sea. *Mar. Pet. Geol.*, **2005**, *22(5)*, 613-621.

42. Hensen, C.; Zabel, M.; Pfeifer, K.; Schwenk, T.; Kasten, S.; Riedinger, N.; Schulz, H.D.; Boetius ,A. Control of sulfate pore-water profiles by sedimentary events and the significance of anaerobic oxidation of methane for the burial of sulfur in marine sediments. *Geochim. Cosmochim. Acta*. **2003**, *67(14)*, 2631-2647.

43. Cai, W.J.; Dai, M.H.; Wang, Y.C.; Zhai, W.D.; Huang, T.; Chen, S.T.; Zhang, F.; Chen, Z.Z.; Wang, Z.H. The biogeochemistry of inorganic carbon and nutrients in the Pearl River estuary and the adjacent Northern South China Sea. *Cont. Shelf Res.* **2004**, *24(12)*, 1 301-1 319.

44. Zhong, J. Preliminary study on zonation of neotectonics and regional stability in Nansha Islands. *Donghai Mar. Sci.* **1998**, *16(01)*, 3-5.

45. Jin, S.; Zhang.L.; Zhong, Z. Q.; Zhou, H. W.; Xiang, H.; Zeng, W.; Liu, R. Geochemical characteristics of the neoproterozoic metavolcanic rocks in Zhejiang and Fujian provinces and its geological significance. *J. Miner. Petrol.* **2008**, *28(01)*:97-105.

46. Yang, S.L. Characteristics of suspended silt at flood period in waters around Songyu, Xiamen. *J. Appl. Oceanogr.* **1990**, *9(04)*, 309-315.

47. Cao. C.; Cai, F.; Li, Y.; Zheng, Y.L.; Wu, C.Q.; Lu, H.Q.; Bao, J.J.; Xu, Y. Characteristics of the Submarine Topography and its Profile Type of the Coast of China. *Acta Geol. Sin.-Engl. Ed.* **2013**, *87(6)*, 1227-1240.

48. Wu, Z.J.; Ren, D.Z.; Zhou, H.Y.; Gao, H; Li, J.T. Sulfate reduction and formation of iron sulfide minerals in nearshore sediments from Qi'ao Island, Pearl River Estuary, Southern China. *Quat. Int.* **2017**, *452*, 137-147.

49. Xu, F.J.; Chen, S.Y.; Qiu, L.W.; Cao, Y.C. A preliminary reassessment of δEu N-ΣREEs plot for distinguishing sediment provenances. *J. Rare Earths.* **2012**, *30(01)*, 94-96.

50. Xu, F.J.; Li, A.C.; Li, T.G.; Xu, T.G.; Chen, S.Y.; Qiu, L.W.; Cao, Y.C. Rare earth element geochemistry in the inner shelf of the East China Sea and its implication to sediment provenances. *J. Rare Earths.* **2011**, *29(07)*, 702-709.

51. Ma, X.H.; Han, Z.Z.; Bi, S.P.; Hu, G.; Zhang, Y.; Xu, C. F. Heavy mineral composition in surface sediments of the Minjiang River estuary and its implications for provenance. *Mar. Geol. Quat. Geol.* **2018**, *38(1)*, 87-95.

52. Ding, H.; Yao, S.P.; Chen, J. Authigenic pyrite formation and re-oxidation as an indicator of an unsteady-state redox sedimentary environment: evidence from the intertidal mangrove sediments of Hainan Island, China. *Cont. Shelf Res.* **2014**, *78(3)*. 85-99.

53. Dong, L.X.; Su, J.L.; Wong, L.A.; Cao, Z.Y.; Chen, J.C. Seasonal variation and dynamics of the Pearl River plume. *Cont. Shelf Res.* **2004**, *24(16)*, 1761-1777.

54. Paul, C.K.; Ussler, III.W.; Holbrook, W.S. Origin of pockmarks and chimney structures on the flanks of the Storegga Slide, offshore Norway. *Geo-Mar. Lett.* **2008**, *28(1)*, 43-51.

55. Anderson, T.F.; Raiswell, R. Sources and mechanisms for the enrichment of highly reactive iron in euxinic Black Sea sediments. *Am. J. Sci.* **2004**, *304(3)*, 203-233.

56. Weber, A.; Jørgensen, B.B. Bacteria sulfate reduction in hydrothermal sediments of the Guaymas Basin, Gulf of California, Mexico. *Deep-Sea Res. Part I-Oceanogr. Res. Pap.* **2002**, *49(5)*, 827-841.

57. Hinrichs, K.U.; Hayes, J.M.; Sylva, S.P.; Brewer, P.G.; DeLong, E.F. Methane consuming archaebacteria in marine sediments. *Nature.* **1999**, *398(6730)*, 802-805.

58. Alongi, D.M.; McKinnon, A.D. The cycling and fate of terrestrially-derived sediments and nutrients in the coastal zone of the Great Barrier Reef shelf. *Mar. Pollut. Bull.* **2005**, *51(1-4)*, 239-252.

59. Harrison, P.J.; Yin, K.; Lee, J.H.W.; Gan, J.P.; Liu, H.B. Physical-biological coupling in the Pearl River Estuary. *Cont. Shelf Res.* **2008**, *28(2)*, 1405-1415.

60. Chatterjee, S.; Dickens, G.R.; Bhatnagar, G.; Chapman, W.G.; Dugan, B.; Snyder, G.T.; Hirasaki, G.J. Pore water sulfate, alkalinity, and carbon isotope profiles in shallow sediment above marine gas hydrate systems: A numerical modeling perspective. *J. Geophys. Res.-Solid Earth.* **2011**, *116(B9103)*, 1-25.

61. Komada, T.; Burdige, D.J.; Li, H.L.; Magen, C.; Chanton, J.P.; Cada, A.K. Organic matter cycling across the sulfate-methane transition zone of the Santa Barbara Basin, California Borderland. *Geochim. Cosmochim. Acta.* **2016**, *176(1)*, 259-278.

62. Meister, P.; Liu, B.; Ferdelman, T.G.; Jørgensen, B.B.; Khalili, A. Control of sulphate and methane distributions in marine sediments by organic matter reactivity. *Geochim. Cosmochim. Acta.* **2013**, *104(1)*, 183-193.

63. Borowski, W.S.; Paull, C.K.; Ussler, W. Global and local variations of interstitial sulfate gradients in deep water, continental margin sediments: Sensitivity to underlying methane and gas hydrates. *Mar. Geol.* **1999**, *159*, 131-154.

64. Kvenvolden, K.A.; Lorenson, T.D. Methane and other hydrocarbon gases in sediments from the southeastern North American continental margin. In: Paull C K, Matsumoto R, Wallace P

J et al, eds. Proceedings of the Ocean Drilling Program , Scientific Results. College Station, Texas: *Ocean Drilling Program*. **2000**, 29-36.

65. Lim, Y.C.; Lin, S.; Yang, T.F.; Chen, Y.G.; Liu, C.S. Variations of methane induced pyrite formation in the accretionary wedge sediments offshore southwestern Taiwan. *Mar. Pet. Geol.* **2011**, *28(10)*, 1829-1837.

66. Torres, M.E.; Mix, A.C.; Rugh, W.D. Precise δ^{13}C analysis of dissolved inorganic carbon in natural waters using automated headspace sampling and continuous-flow mass spectrometry. *Limnol. Oceanogr. Meth.* **2005**, *3(8)*, 349-360.

67. Kraal, P.; Burton, E.W.; Bush, R.T. Iron monsulfide accumulation and pyrite formation in eutrophic estuarine sediments. *Geochim. Cosmochim. Acta*. **2013**, *122(1)*, 75-88.

68. Peng, Y.S.; Chen, G.Z.; Tian, G.H.; Yang, X.B. Niches of plant populations in mangrove reserve of Qi'ao Island, Pearl River Estuary. *Acta. Ecolog. Sin.* **2009**, *29(6)*, 357-361.

69. Pohlman, J.W.; Riedel, M.; Bauer, J.E.; Canuel, E.A.; Paull, C.K.; Lapham, L.; Grabowski, K.S.; Coffin, R.B.; Spence, G.D. Anaerobic methane oxidation in low-organic content methane seep sediments. *Geochim. Cosmochim. Acta.* **2013**, *108(1)*, 184-201.

70. Iversen, N.; JØrgensen, B.B. Anaerobic methane oxidation rates at the sulfate-methane transition in marine sediments from Kattegat and Skagerrak (Denmark). *Limnol. Oceanogr.* **1985**, *30(5)*. 944-955.

71. Hurtgen, M.; Lyons, T.W.; Ingall, E.D.; Cruse, A.M. Anomalous enrichments of iron monosulfide in euxinic marine sediments and the role of H_2S in iron sulfide transitional zones: examples from Effingham Inlet, Orca Basin, and the Black Sea. *Am. J. Sci.* **1999**, *299(7)*, 556-588.

72. Mazumdar, A.; Paropkari, A.L.; Borole, D.V.; Rao, B.R.; Khadge, N.H.; Karisiddaiah, S.M.; Kocherla, M.; Joäo, H.M. Pore-water sulfate concentration profiles of sediment cores from Krishna-Godavari and Goa basins, India. *Geochem. J.* **2007**, *41(4)*, 259-269.

73. Morgan, B.; Rate, A.W.; Burton, E.D. Water chemistry and nutrient release during the resuspension of FeS-rich sediments in a eutrophic estuarine system. *Sci. Total Environ.* **2012**, *432*, 47-56.